Fabrication of nanocomposite powders with a core-shell structure

Binling Chen*, Bahareh Yazdani, Luiza Benedetti, Hong Chang, Yanqiu Zhu, Oana Ghita

College of Engineering, Mathematics and Physical Sciences, University of Exeter, Exeter, EX4 4QF, UK

ARTICLE INFO

ABSTRACT

This study presents a new process for producing nanocomposite powders for use in various manufacturing processes such as laser sintering or dry powder impregnation techniques for thermoplastic composites manufacture. Polyetherimide (PEI) was used as a polymeric coating/shell to encapsulate nanoparticles on the surface of poly ether ether ketone (PEEK) particles, which were used as a core matrix. Nanoparticles with different morphologies, known to enhance thermal and electrical performance of polymers: 2D graphene nanoplatelets (GNPs) and inorganic fullerene-like tungsten disulfide (IF-WS$_2$) in different concentrations (0.1, 1, and 5 wt%) were incorporated in the shell structures. The coated powders had approximately the same particle size distribution as the uncoated, plain powders, which is an indication that the shell was in nm size and the coating process did not affect the overall size of the particles. Furthermore, the core-shell particles exhibit a smoother surface and an improved flowability after coating. The Transmission Electron Microscopy (TEM) images of the nanocomposite particles cross-section area confirmed the formation of core-shell structure, and the presence of the nanoparticles embedded into the shell layer. The scanning electron microscopy (SEM) images showed a homogeneous distribution of nanoparticles within the coating layer at lower nanoparticle concentrations (0.1 and 1 wt%).

1. Introduction

Polymer based nanocomposites are known to have enhanced characteristics such as good mechanical properties, electrical conductivity, thermal stability and chemical resistance due to the nanoparticles added. For example, carbonaceous nanofillers such as carbon nanotubes and graphene exhibit high mechanical strength [1]. Studies showed that carbon nanotubes can reach a tensile modulus of 1 TPa, tensile strength of 50–150 GPa with a failure strain in excess of 5% [2,3]; graphene nanosheet measured a Young's modulus of 1 TPa, ultimate strength of 130 GPa, a specific area of 2600 m^2/g [4], a high electric conductivity of 6000 S/cm [5], and a high thermal conductivity of ∼5000 W/mK [6]. Inorganic nanofillers such as tungsten oxide (WO$_x$) and tungsten disulphide (WS$_2$) have a wide range of interesting properties. WO$_x$ are known to exhibit chromogenic characteristics [7] and inorganic fullerene-like tungsten disulphide (IF-WS$_2$) recorded shockwave-absorbing properties [8].

The quality of the dispersion of nanoparticles into polymers is one key issue frequently mentioned as a challenge in the nanocomposite processing [9]. One practical method for dispersing nanofillers into thermoplastic polymeric matrices is direct melt compounding [10–12]. However, it is difficult to achieve uniform dispersion especially at high loadings due to the extremely high surface activity of nanofillers which makes the particles aggregate tightly, generating micron-sized clusters [9] and high viscosity of thermoplastic matrices. The formation of impurities and porosity is sometimes encountered, which can result in the composites having impaired properties compared to those of the virgin polymer. If the nanocomposites are required in powder form (for example, for laser sintering, dry powder impregnation and hot compression moulding) the melt compounding process is followed by milling. This process is costly and ineffective due to the high energy consumption required to achieve substantial amounts of material at appropriate particle size distributions. In addition, the success of milling depends on the intrinsic properties of the polymer such as toughness and the applied milling method [13,14].

Appropriate chemical and physical methods to achieve controlled dispersion of nanoparticles were developed [15]. Functionalization of nanoparticles, using weak interactions, ionic interactions, or covalent functionalization, is one of the strategies. The use of surfactants was applied sometimes to help efficient dispersion of nanoparticles [16,17]. "Grafting-to" the nanoparticles with functional polymers and "Grafting-from" the nanoparticles with radical groups through condensation, ring opening or controlled polymerization processes is another strategy [18,19]. However, both of these strategies are not fully scaled up to

---

allow use in continuous larger processes.

In the case of laser sintering, dispersion of nanoparticles into polymeric powders as dry mixtures had been studied as a more cost-effective method [20], but it was noticed that it may lead to agglomeration and poor dispersion when percentages increase. In addition, the handling of dry-mixed powders poses significant health and safety concerns.

Mo et al. presented a novel method to attach nanoparticles to the surface of the polymeric particles by softening the surface of the particle with the help of a selective liquid under specific temperatures and pressures [21]. This preparation method was demonstrated on nylon particles with CNTs at 0.1% by weight. His study focused on laser sintering only [22–24]. The SEM results showed nanofillers homogenously distributed on the surface of the particles [22]. However, this method is not suitable for high temperature polymers, due to the low boiling point (bp) of the selective liquid (bp < 200 °C). Therefore, this process is limited to engineering polymers with lower bps.

When it comes to nanoparticle reinforced composites, known as hierarchical composites, most studies have focused on thermoset composites [25]. Nanoparticles have been added to thermoset composites to improve delamination resistance, through-thickness performance and increase the matrix toughness. Such techniques are difficult to replicate with thermoplastics due to their increased viscosity even at melt temperatures. In the case of thermoplastic composites other fabrication methods are preferred such as dry powder impregnation, fibre comingling or film stacking. In this area, the majority of the studies to date have focused on film stacking. For example, one study examined the properties of $IF-WS_2$/iPP (polypropylene)/GF (glass fibre) composites by incorporating $IF-WS_2$ nanoparticles into the iPP matrix through melt compounding as well as film fabrication, alternating iPP/$IF-WS_2$ films with layers of GF [26]. In a different study, $CaCO_3$ micro-particles and nanoclay were melt compounded into a PP matrix. The micro and nano reinforced matrix was used in the film stacking manufacturing method for producing thermoplastic laminates [27]. Studies attempting the addition of nanoparticles into a dry powder impregnation process for hybrid thermoplastic composites are rare, possibly due to the difficulties of fabricating suitable composite powders.

As thermoplastic composites are becoming more and more attractive to aerospace and automotive industries due to their high strain-to-failure, increased fracture toughness, better impact tolerance, shorter moulding cycles, recyclability and repairability, the need for high performance polymers with enhanced functionalities for complex shape manufacture such as laser sintering or conventional manufacture of hybrid and hierarchical structures is expected to grow [28]. In this paper, we demonstrate an alternative method to fabricate nanocomposite powders with high performance polymers such as PEEK. A core-shell structure is designed, where the shell, a thin layer of a specific polymer (in this case PEI) traps the nanoparticles on the surface of a plain PEEK particle, which represents the core. The chosen core particle was PEEK, which has already been used in laser sintering. Therefore, it is proposed that the nanocomposites powders fabricated through this method could be used for laser sintering as well. The manufacturing processes identified here are not trialled in this study; they will form the basis of a different paper.

The composition of the prepared powders was characterized by X-Ray Diffraction (XRD). The surface morphology was observed by Scanning Electron Microscopy (SEM), and the particle size distribution (PSD) was measured for the powders before and after coating with and without nanomaterials. The core-shell structures were further confirmed by Transmission Electron Microscopy (TEM). The effect of PEI coating (thickness and wt%) had been examined using differential scanning calorimetry (DSC). The initial powder rheology tests showed that PEI coated PEEK and its $IF-WS_2$ nanocomposite powders have improved flowability when compared with the pure PEEK powders. This type of nanocomposite powders are expected to achieve a better homogeneous distribution in a nanocomposite than the conventional

melt compounding when applied in manufacturing processes as those mentioned above.

2. Experimental

2.1. Materials

The materials used in this study have been divided into three types: (1) thermoplastic core particle; (2) thermoplastic shell/coating; (3) nanoparticles. The commercial EOS HP3 PEK powder, the only commercial high temperature laser sintering powder, was used for benchmarking during powder rheology analysis.

(1) PEEK 150PF powder, supplied by Victrex, was used for the core particles.
(2) Polyetherimide (PEI) was purchased from Sigma-Aldrich to be used as coating.
(3) Graphene nanoplatelets (GNPs) were purchased from Thomas Swan & Co Ltd, and $IF-WS_2$ (inorganic fullerene-like tungsten disulphide) nanoparticles were produced in house, following the process defined in the literature [29].

2.2. Preparation of the core-shell particles without nanoparticles

2.2.1. PEI coated PEEK powders (referred to as PEI/PEEK)

PEI granules were dissolved in dichloromethane. PEEK powders were then added to the PEI solution. Following a strong ultrasonic treatment (Qsonica sonicator Model Q125) and careful removal of the solvents, the collected powders were dried in an oven at 80 °C for 24 h. The dried powders were gently ground to break down any agglomeration which was formed during drying. The PEI was added at 15 wt% of the total amount of PEI and PEEK into the solvent. Other PEI concentrations were also prepared: 0.1, 1, 50 wt%. For clarification, unless specified, the PEI coated PEEK (PEI/PEEK) powder mentioned in the paper refers to 15 wt% PEI to PEEK.

2.3. Preparation of the core-shell particles with nanoparticles (referred to as GNP-PEI/PEEK and WS_2-PEI/PEEK)

The process was similar to the preparation of the PEI coated PEEK. Nanoparticles were added after PEI was fully dissolved and prior to adding PEEK particles.

2.4. Fabrication of GNP-PEI/PEEK composites by hot-compression moulding

Films of pure 150PF PEEK, PEI/PEEK, $1WS_2$-PEI/PEEK, and $5WS_2$-PEI/PEEK powders were made using a Lab Tech LP-S-50 hydraulic press. Powders were evenly spread in the mould. The mould was then transferred to the hot-press machine. The pressure was set at 15 bar, and the heating temperature was set as 400 °C. The pre-heating time was 5 min; the pressing & venting time was 2 min; the full pressing time was 5 min; and the cooling time was 30 min.

2.5. Characterizations

2.5.1. X-ray diffraction (XRD)

X-ray diffraction (XRD) patterns were measured by an X-ray Diffractometer (Bruker D8 Advance) with a Cu Kα radiation at 40 kV and 40 mA. Powdered samples were spread flatly on a glass side, and they were measured at a step time of 1 s and a step size of 0.02°.

Semi-quantitative (SQ) analysis was conducted using the evaluation Bruker software (EVA) based on the relative intensities of nanomaterials in the polymer matrix. The 5GNP-PEI/PEEK and $5WS_2$-PEI/PEEK powders were used as calibration values to obtain I/I_{cor} for each type of composite powders (I/I_{cor} is known as a ratio between the intensities of
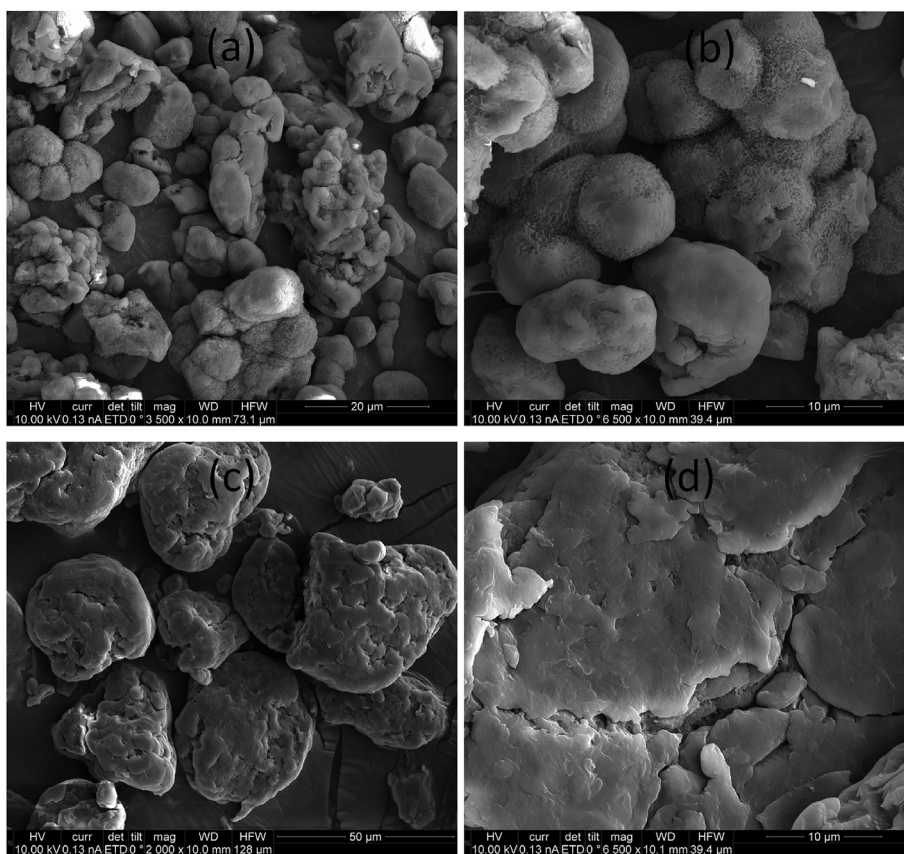
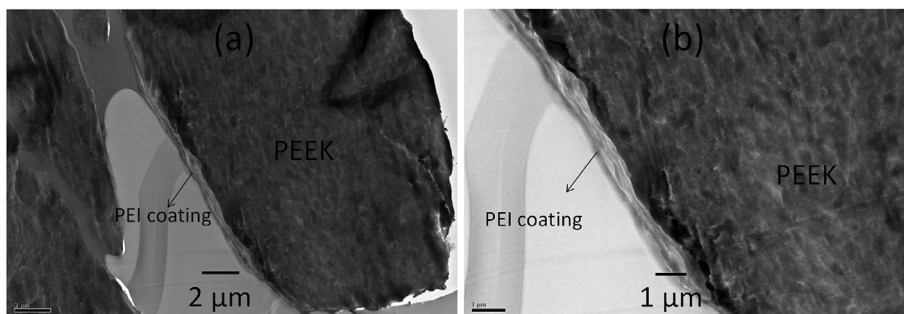**Fig. 1.** SEM images of (a), (b) 150PF PEEK powder; and (c), (d) PEI coated PEEK (PEI/PEEK) powder.

Fig. 2. TEM images of cross-section area of PEI coated PEEK (PEI/PEEK) powder.

the strongest line of interest and the strongest line of corundum). The I/I_{cor} value of PEI/PEEK, came out as 0.227 and 1.985, respectively, in GNP-PEI/PEEK and WS$_2$-PEI/PEEK powders. Then the contents of GNP and WS$_2$ in the GNP-PEI/PEEK and WS$_2$-PEI/PEEK composite powders were calculated automatically in EVA software. Three repeats were performed on each type of nanocomposite powder and average values were used for comparison and discussion.

2.5.2. Scanning electron microscopy (SEM)

SEM images were recorded using a Nova Nanolab 600 scanning electron microscope in a high vacuum mode, at an acceleration voltage of 20 kV. Powdered samples were spread and pasted on a conductive carbon double-sided tape. A thin layer of gold coating (ca. 7 nm) was sputtered onto the samples to reduce charging. All the powders prepared were examined using SEM.

2.5.3. Transmission Electron Microscopy (TEM)

TEM was used to investigate the presence and distribution of the

nanoparticles within the coating/shell of the nanocomposite powders as described in section 2.2. Samples were prepared by mixing a small amount of powdered sample with Spurr Resin (TAAB Laboratories, Aldermaston, UK) in a 1:1 proportion. This mixture was placed in a plastic capsule and filled with Spurr Resin, and was polymerized at 60 °C overnight. Using an RMC POWERTOME PC Ultracut, 70 nm ultrathin sections were obtained and collected on pioloform-coated EM 100 mesh copper grids (Agar Scientific, Stansted, UK). These sections were imaged using a JEOL JEM 1400 TEM operated at 120 kV and an ES 100 W CCD digital camera (Gatan, Abingdon, UK).

Nanoparticles (GNPs and IF-WS$_2$), GNP-PEI/PEEK and WS$_2$-PEI/PEEK were also examined using TEM. The TEM images were obtained using a JOEL-2100 TEM at a voltage of 200 kV. The nanoparticle powders were first dispersed in isopropyl alcohol under sonication for 20 min, then pipetted onto a holey carbon Cu grid to form TEM specimens.
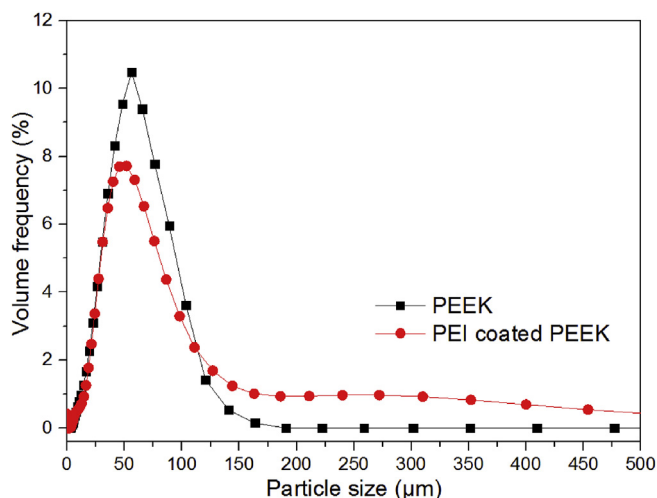
Fig. 3. Particle size distribution of pure 150PF PEEK and PEI coated PEEK powders.
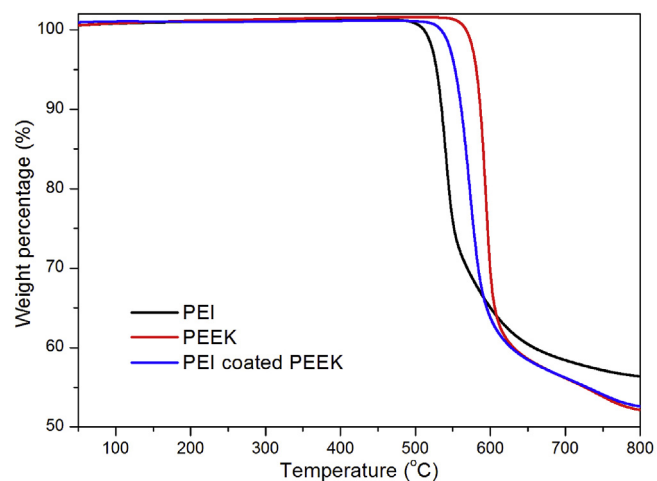

Fig. 4. TGA of pure 150PF PEEK, PEI, and PEI coated PEEK powders.

2.5.4. Particle size distribution (PSD)

The particle size distribution of PEEK 150PF and PEI/PEEK powders were measured using Malvern Instruments Masterisizer. The powdered samples were first suspended in a 0.4% sodium hexametaphosphate water solution. The particle size distribution can then be measured by detecting the light scattering pattern of the powdered samples in the prepared solution.

2.5.5. Differential scanning calorimetry (DSC)

A Mettler Toledo DSC 821e/700 was used to measure melting and crystallisation temperatures, glass transition temperature and to determine the degree of crystallinity. Nitrogen with a flow rate of 50 ml min^{-1} was used as protective gas. The powdered samples were heated in the DSC from 25 °C to 420 °C with a heating rate of 10 °C min^{-1}. Three repeat measurements were carried out. The enthalpy values used for the calculation of crystallinity were corrected to consider the PEI content using the equation below:

$$\Delta H_{corr} = \Delta H / [(1 - x)]$$

where ΔH_{corr} is the corrected enthalpy (J g^{-1}); ΔH is the normalized enthalpy of the transition (J g^{-1}); x is the fraction of PEI in the composite powders [30]. PEI is an amorphous polymer therefore it is not contributing to the crystallisation process but can influence and therefore reduce crystallisation [31].
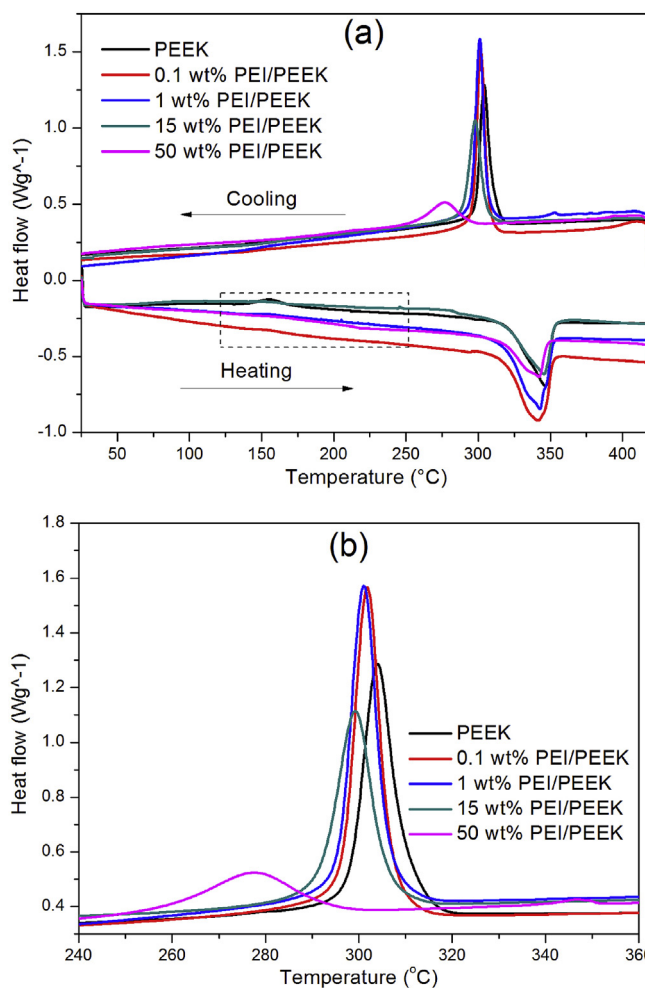

Fig. 5. (a) DSC thermograms and (b) Cooling phase of virgin PEEK and powders with various PEI concentrations.

Table 1

Thermal properties of virgin PEEK and powders with various PEI concentrations including melting temperature (T$_m$); crystallisation temperature (Tc); measured enthalpy of crystallisation (ΔH_c); normalized enthalpy of crystallisation corrected for PEI content (ΔH_c corr.); PEEK crystallinity (X$_c$).

wt % PEI	T$_m$ °C	T$_c$ °C	ΔH_c J g^{-1}	ΔH_c corr. J g^{-1}	X$_c$ %
0	347.2 ± 0.2	304.0 ± 0.2	56.6 ± 0.1	56.6 ± 0.1	43.5 ± 0.1
0.1	342.4 ± 0.6	301.7 ± 0.1	58.8 ± 0.6	58.9 ± 0.6	45.3 ± 0.4
1	342.8 ± 0.5	301.1 ± 0.1	57.4 ± 0.6	57.9 ± 0.6	44.6 ± 0.5
15	346.1 ± 0.4	298.7 ± 0.7	46.7 ± 04	51.9 ± 0.5	39.9 ± 0.4
50	342.0 ± 0.1	277.3 ± 0.4	24.9 ± 0.4	49.7 ± 0.8	38.2 ± 0.6

2.5.6. Thermogravimetric analysis (TGA)

In order to determine the exact wt% of PEI onto PEEK, TGA tests of PEI, PEEK, PEI coated PEEK were performed from 30 to 800 °C at 10 °C min^{-1} under nitrogen atmosphere with a flow of 50 ml min^{-1}.

2.5.7. Powder rheology test

A Freeman FT-4 powder rheometer was used to assess powder flow properties. The tests carried out here (stability and flow rate) aim to assess the stability and flow properties of the powders. These tests were performed in a 25 ml split vessel filled with powder in a pre-conditioned state. The conditioned bulk density (CBD) was measured at this stage, in which any external effect can be neglected and the volume was
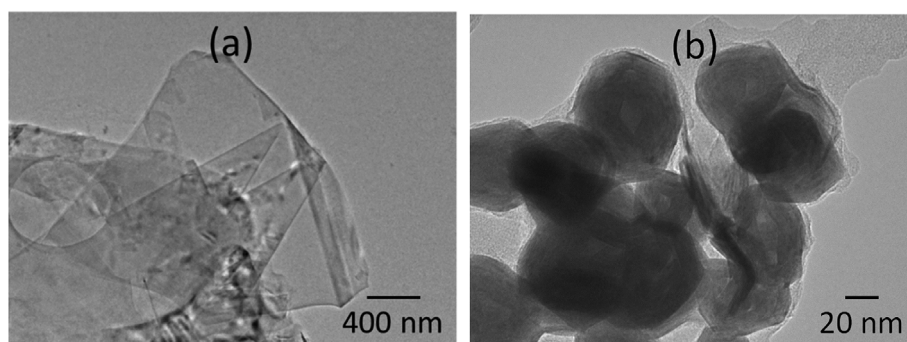
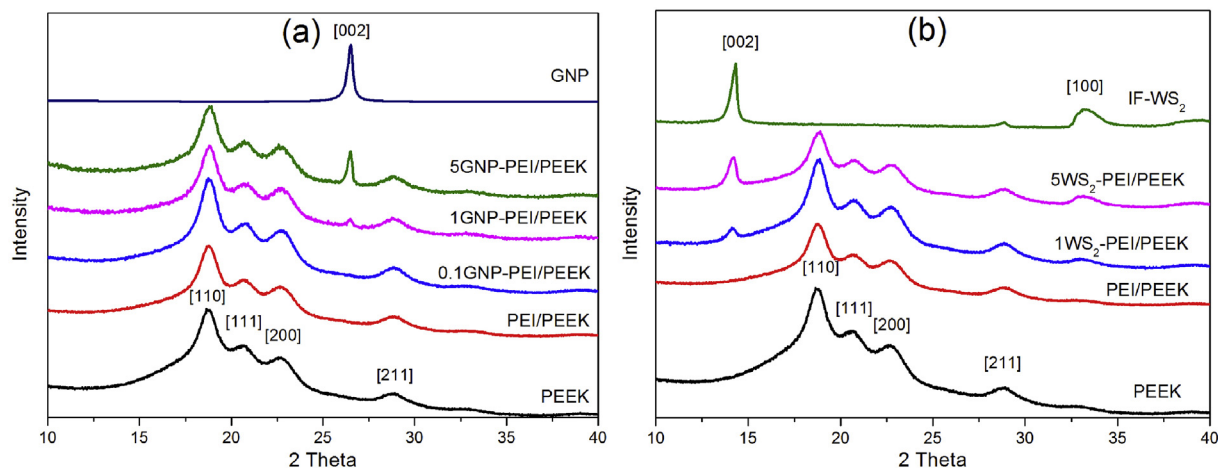**Fig. 6.** TEM images of (a) GNP; (b) IF- WS$_2$ nanoparticles.

Fig. 7. XRD patterns of (a) GNP-PEI/PEEK powders; (b) WS$_2$-PEI/PEEK powders.

constrained to 25ml. A blade applied a torque by rotating counter-clockwise at 100 mm/s whilst moving downwards. The standard methodology consists of repeating this movement for seven times; the average energy required to perform one rotation at the last repeat divided by the average energy required to perform one rotation in the first repeat gives a factor known as the Stability Index (SI). After this stage was completed, the speed of the blade was gradually reduced from 100 mm/s until it reached 10 mm/s. The Basic Flowability Energy (BFE) was measured in the 7th cycle of the blade rotating downwards at 100 mm/s, whilst the Specific Energy (SE) was calculated by performing the average of energy applied to lift the blade by rotating it upwards at the 6th and 7th rotation at 100 mm/s. The BFE provides information regarding the difficulty on displacing the powder in an unconfined state and is frequently associated with powder cohesivity, morphology and packing. The Specific Energy (SE) measures the capability of lifting the powder from the bottom of the vessel to the top in an unconfined state. The SE provides information of size, shape and surface texture of the particles and is an indication of mechanical interlocking and friction. A combination of both BFE and SE results give a better understanding of powder flow: high values of BFE combined with low values of SE suggest a better flow performance as well as a uniform packing.

2.5.8. Dynamic thermo-mechanical analysis (DMTA)

A Mettler Toledo DMA-1 was used to measure the hot compression moulded films. All specimens were cut in the following dimensions: 30 * 7 * 0.5 mm^3. All samples were tested in a three-point bending mode with a frequency of 1 Hz and a strain displacement of 10 μm. Each sample was heated from 30 to 260 °C with a heating speed of 3 °C min^{-1}. DMTA was selected to investigate the viscoelastic behaviour of materials. Storage modulus (E′), loss modulus (E″) and Damping factor

(Tanδ) were examined. Three repeats of each material were carried out.

3. Results and discussion

3.1. Structure evaluation of PEI/PEEK

The surface morphology of pure 150PF PEEK, and PEI coated PEEK powders were examined by SEM. The pure PEEK particles have a rough surface with granular and fibrous structures (see Fig. 1a–b), consistent with the previous powder studies of PEEK [32,33]. The particle surface of the coated PEEK particles became smoother, making the new particles rounder (see Fig. 1c–d). Results in Fig. 1 suggest that PEI successfully coated the surface of PEEK particles. The SEM observations are confirmed by the TEM images shown in Fig. 2, which represent cross-sectional areas of PEI coated PEEK. A uniform and thin coating layer with thickness of less than 500 nm covered the whole surface of PEEK particles and it can be observed in Fig. 2.

Particle size distributions (PSD) of pure 150PF PEEK and PEI/PEEK powders were measured in order to study the effect of the coating on the pure PEEK powders. As shown in Fig. 3, pure 150PF PEEK exhibits a particle size distribution ranging between 1 and 150 μm with the highest volume frequency centred at approximately 60 μm. The PEI/PEEK powder has a wider distribution (slightly bimodal) with a peak centred at 50μm and one appearing at approximately 275 μm. This may be due to the aggregation of PEEK powders with PEI during solvent removal process. However, it is believed that the presence of this peak can be removed easily through a further short deagglomeration process.

The TGA curves of 150PF PEEK, PEI and PEI coated PEEK powders are shown in Fig. 4. 150PF PEEK, PEI and PEI coated PEEK powders started to decompose at 545, 485, and 515 °C, respectively. Based on their residual weight percentage at 800 °C, the actual PEI wt% in PEI
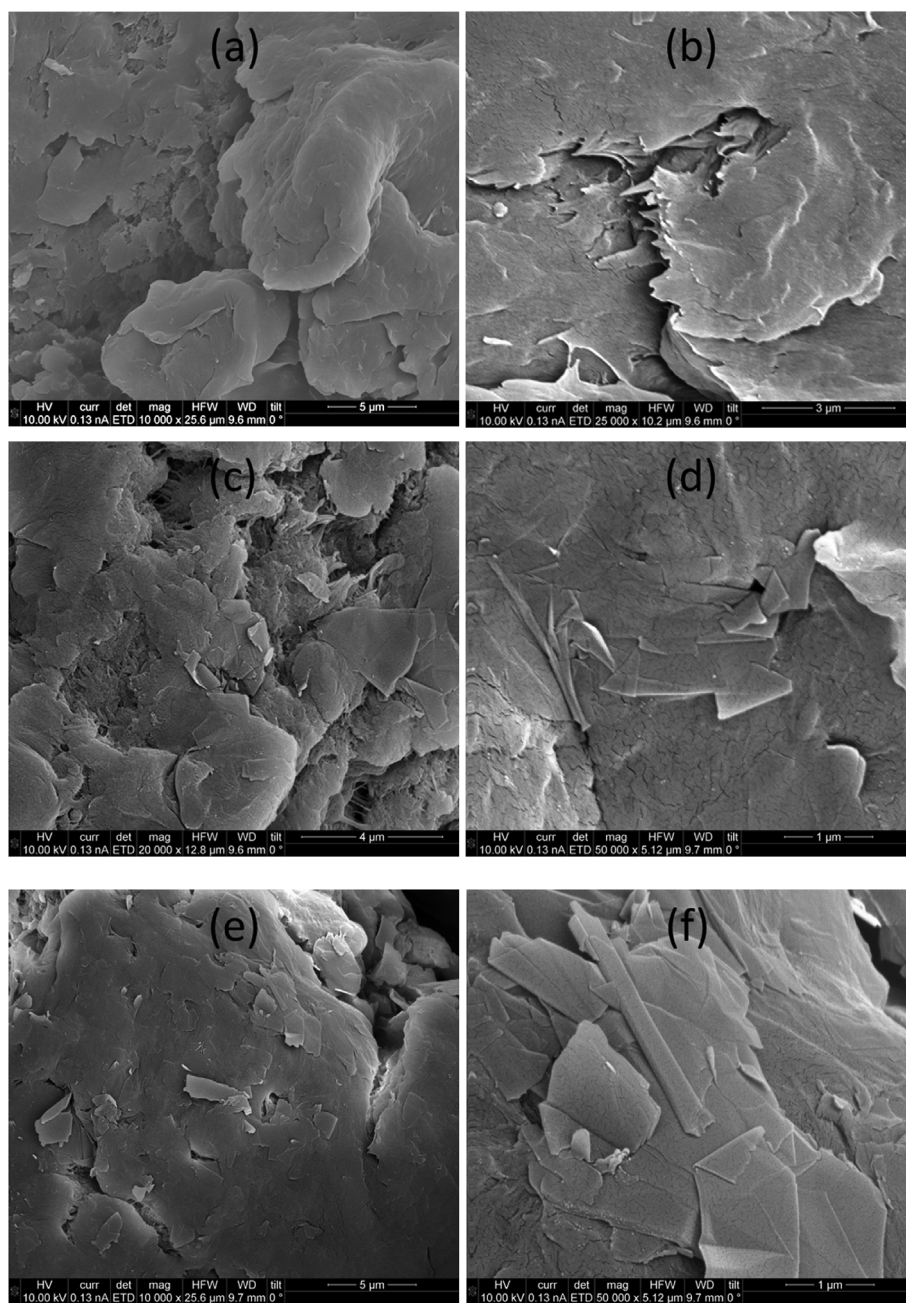
Fig. 8. SEM images of (a, b) 0.1GNP-PEI/PEEK powders; (c, d) 1GNP-PEI/PEEK powders; and (e, f) 5GNP-PEI/PEEK powders.

coated PEEK powder was calculated as 15.7 wt%, which is consistent to the original weight percentage of 15 wt%.

The effect of PEI concentration on the particles was also examined by TEM. Fig. S1 shows the TEM images of cross-sectional areas of powders with different PEI contents. For very small amounts of PEI (0.1 and 1 wt%), the coating was not uniform, where at a very high concentration (50 wt%), the PEI wrapped the PEEK particles completely. Only 15 wt% PEI/PEEK powders had a uniform PEI coating, as discussed above.

The DSC thermograms of the powders are included in Fig. 5a. For clarity, Fig. 5b presents the cooling phase of the powder thermographs. In Fig. 5a, the region highlighted by the dotted box shows the glass transition temperature (T_g) region. Except for pure PEEK powder, which presented a T_g at 135 °C, it was very difficult to define the T_g of the blend powders. A closer analysis seems to hint to the presence of two T_g values, but the results at this stage are inconclusive.

Pure PEEK crystallized at 304 °C on cooling from the melt. The crystallisation temperature decreased to 277.3 °C with the increase in PEI content (Table 1), indicating that the crystallisation of PEEK was hindered by PEI [34]. As can be seen from Table 1, the crystallinity of the PEI/PEEK slightly increased with the PEI content (up to 1 wt%), and then decreased with the PEI content (at 15 and 50 wt%), similar to the previous studies [31,35].

Fig. 6 presents the TEM images of GNP and IF-WS$_2$ nanoparticles with uniform particle size, where the particle size of IF-WS$_2$ is around 80 nm. GNPs are stacks of several layers.

3.2. Structural and thermal evaluation of PEI coated PEEK (PEI/PEEK) powders incorporating nanoparticles

The presence of the nanoparticles was checked using XRD, SEM and TEM. The XRD of PEEK presents four typical peaks at 18.8°, 20.8°,

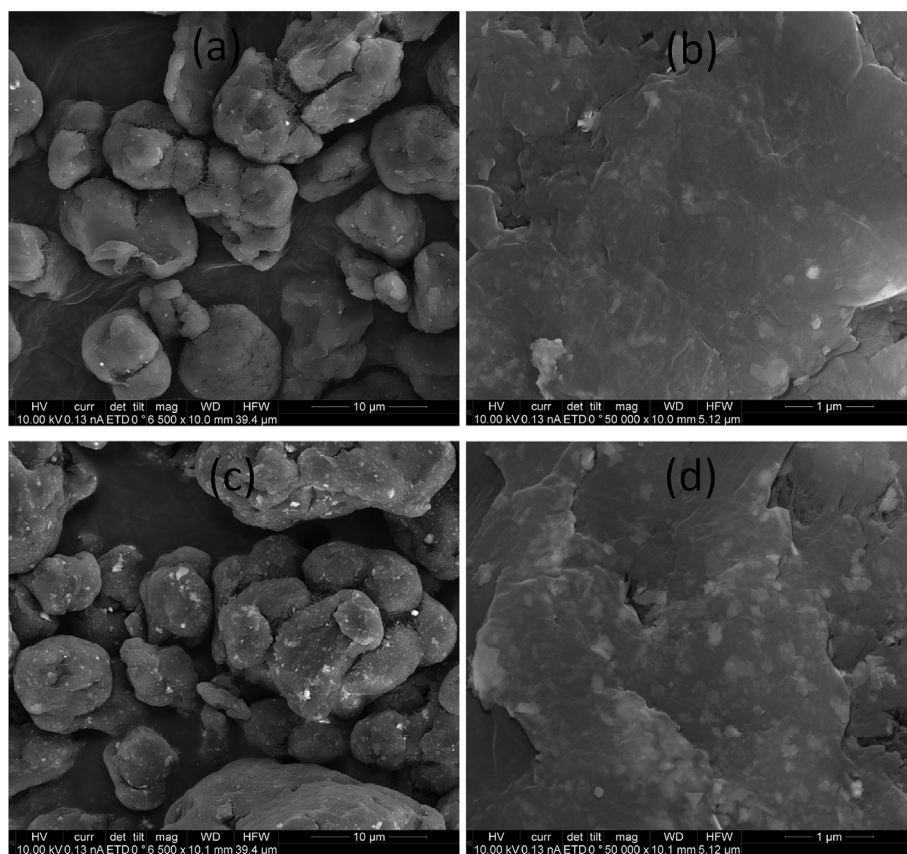**Fig. 9.** SEM images of (a, b) 1WS$_2$-PEI/PEEK; (c, d) 5WS$_2$-PEI/PEEK powders.
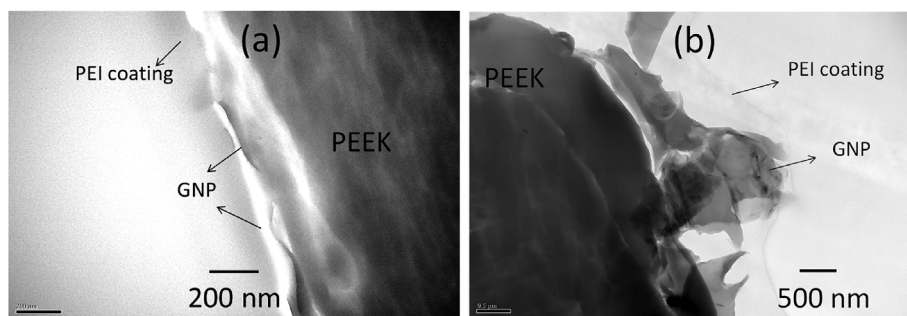

Fig. 10. TEM images of cross-section area of (a) 0.1GNP-PEI/PEEK; and (b) 5GNP-PEI/PEEK powders.

22.8°, and 28.9°, which are attributed to the PEEK crystal planes 110, 111, 200, 211, respectively [36]. As PEI is amorphous, the XRD pattern of PEI/PEEK is similar to that of the pure PEEK. Fig. 7a shows the XRD of PEI/PEEK incorporated with GNP at various GNP contents. GNP has a typical XRD peak at 26.3°, corresponding to the (002) planes of GNP [37]. The intensity of this GNP peak increases with the increase in GNP content in the composite powders. Fig. 7b shows the XRD patterns of PEI/PEEK incorporated with IF-WS$_2$. The peak at around 14.3° corresponds to the (002) plane of IF-WS$_2$ (Fig. 7b) [38]. The XRD peaks of the inorganic nanoparticles appeared in their corresponding composite powders, and the peak intensities increased with the nanoparticles content.

The semi-quantitative XRD results showed a good correlation between the amount of nanomaterials originally added and the wt% incorporated within the shell. Hence, the GNP added at 1 wt% to the PEI/PEEK powder had a similar value of 1.2 ± 0.2 wt% calculated from XRD. Similarly, the 1 wt% WS$_2$ had a calculated value of 1.4 ± 0.3 wt% from XRD. The 0.1 wt% GNP resulted in a similar value from XRD,

however it is less reliable compared to the higher concentrations, as the XRD peak for GNP is within the noise level. Overall the calculated contents were consistent with the original concentrations, indicating a good mixing and no loss of the particles during the fabrication processes.

SEM was used to observe the surface morphology of the GNP-PEI/PEEK. Fig. 8 shows SEM images of GNP-PEI/PEEK powders with different GNP contents (0.1, 1, and 5 wt%). GNP was adhered to the core particles. For 0.1GNP-PEI/PEEK powders (shown in Fig. 8a and b), it is difficult to identify the GNP on the surface of the particles where at higher GNP content (5 wt%) (Fig. 8e and f), an aggregation of GNP was observed; however, the aggregated GNP is still adhered onto the particle surface. Fig. 9 shows the SEM images of 1WS$_2$-PEI/PEEK and 5WS$_2$-PEI/PEEK powders. WS$_2$ nanoparticles can be recognized on the surface of both PEI/PEEK powders, as white speckles.

In order to evaluate how the nanoparticles were embedded into the PEI coating layer, TEM images of cross-section areas of PEI/PEEK incorporating different nanoparticles were taken. Fig. 10 shows TEM
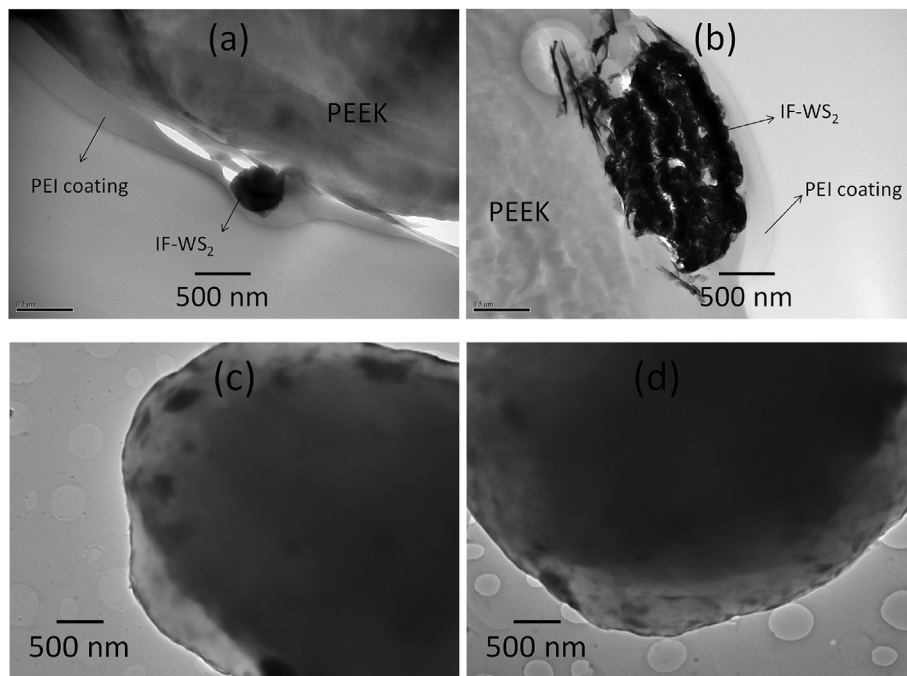
Fig. 11. TEM images of cross-section area of (a) 1WS$_2$-PEI/PEEK; (b) 5WS$_2$-PEI/PEEK powders; TEM images of (c) and (d) 5WS$_2$-PEI/PEEK particle.
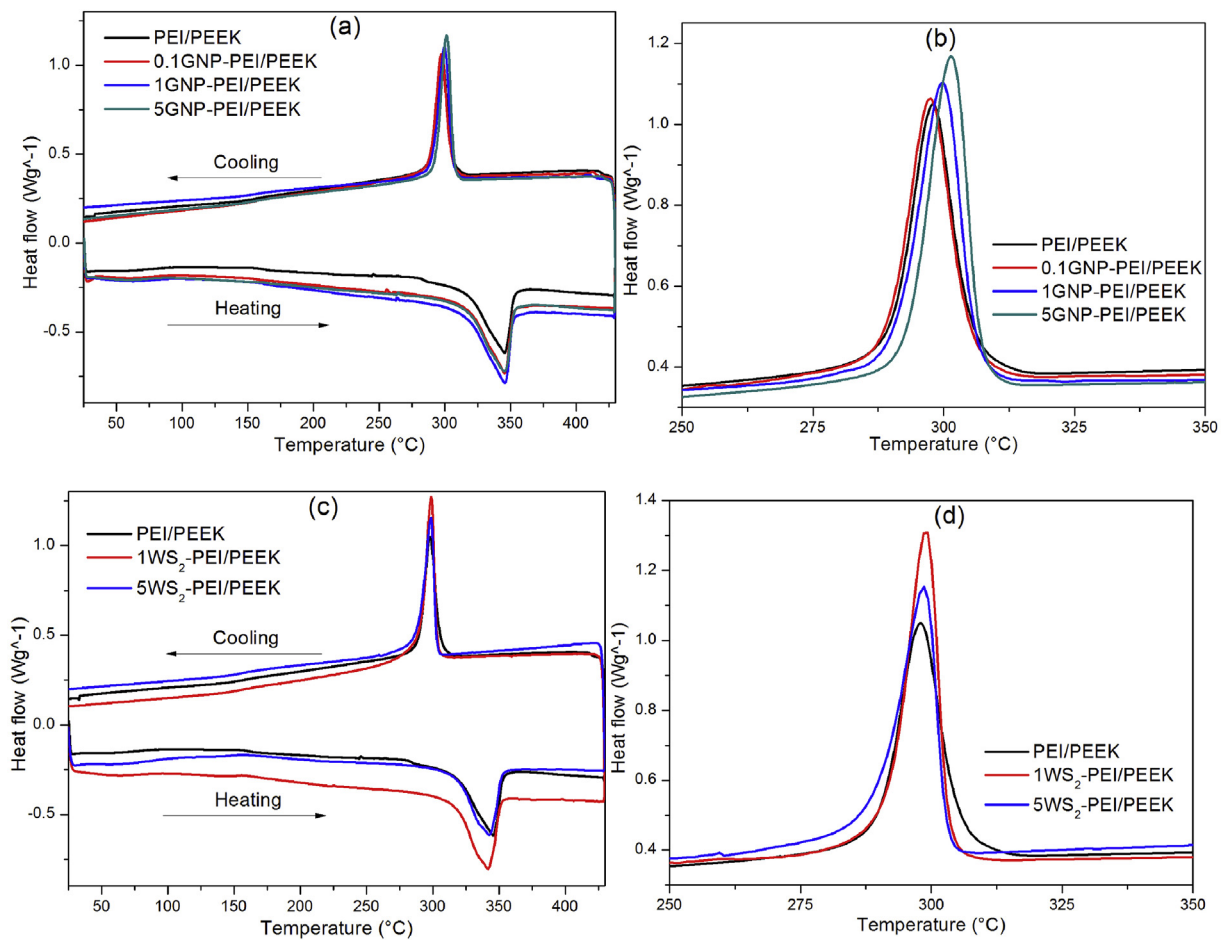

Fig. 12. DSC curves of (a) GNP-PEI/PEEK powders; (b) their zoomed in cooling phase; (c) WS$_2$-PEI/PEEK powders; and (d) their zoomed in cooling phase.
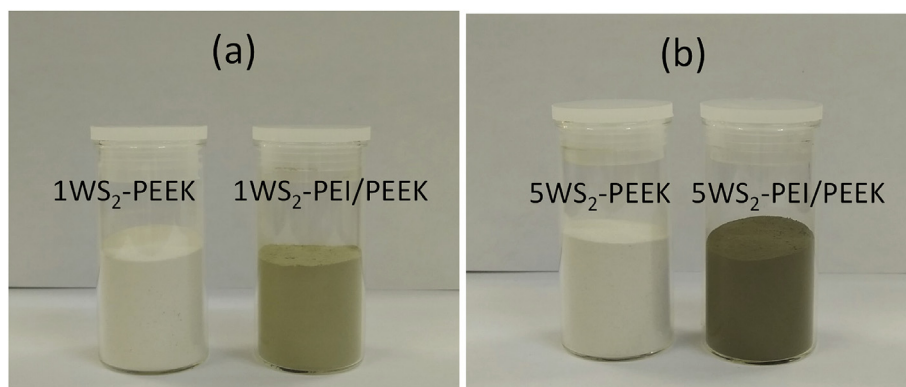
Fig. 13. Digital images of (a) 1WS$_2$-PEEK and 1WS$_2$-PEI/PEEK; (b) 5WS$_2$-PEEK and 5WS$_2$-PEI/PEEK powders.

Table 2
CBD, BFE, SE and SI values of powders obtained from the powder rheology test.

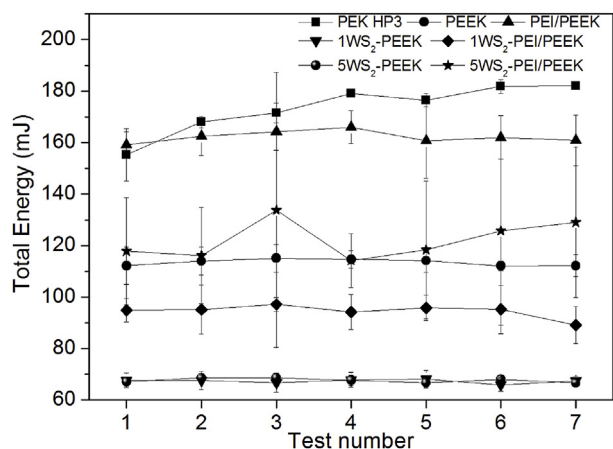| Powders	CBD (g/ml)	BFE (mJ)	SE (mJ/g)	SI
PEK HP3	0.46 ± 0	182.1 ± 0.8	7.2 ± 0.2	1.2 ± 0.1
PEEK	0.41 ± 0	112.2 ± 4.2	6.6 ± 0.1	1.0 ± 0.1
PEI/PEEK	0.50 ± 0	160.9 ± 9.7	6.5 ± 0.4	1.0 ± 0.1
1WS$_2$ – PEEK (dry mix)	0.34 ± 0	67.5 ± 1.7	6.0 ± 0.1	1.0 ± 0.1
5WS$_2$ – PEEK (dry mix)	0.34 ± 0	66.6 ± 1.3	5.7 ± 0.1	1.0 ± 0.1
1WS$_2$ – PEI/PEEK	0.45 ± 0	89.1 ± 7.2	7.0 ± 0.6	0.9 ± 0.1
5WS$_2$ – PEI/PEEK	0.49 ± 0	129.0 ± 29.2	8.6 ± 1.6	1.1 ± 0.4

Fig. 14. Stability test of EOS PEK HP3, pure 150PF PEEK, PEI coated PEEK, 1WS$_2$-PEEK and 5WS$_2$-PEEK (dry mixtures), 1WS$_2$-PEI/PEEK, and 5WS$_2$-PEI/PEEK powders.

images of GNP-PEI/PEEK and WS$_2$-PEI/PEEK powders with various concentrations. The presence of GNP encapsulated in PEI was visible at 0.1 wt% and 5 wt% (see Fig. 10 a and b) when the surface was examined at high magnifications, but it was difficult to observe their distribution over larger areas across individual particles due to the size of the PEEK particles (see Fig. 3 for particle size distribution of PEEK powder). In the case of WS$_2$, the presence of the nanoparticles was clearly observed in all images as shown in Fig. 11.

It is known that nanoparticles can sometimes affect the thermal properties of the matrix by increasing the crystallisation temperature and the rate of crystallisation, or by changing the glass transition temperature or melting temperature [39–42]. For this reason, the thermal behaviour of the nanocomposite powders was also measured. Fig. 12a and b shows that GNP-PEI/PEEK powders exhibited similar thermal behaviour. The melting temperature was similar, while the crystallisation temperature was shifted to higher temperatures with the addition of GNP. This is in agreement with previous studies, which

showed that GNPs act as nucleating points in PEEK [39]. In the case of WS$_2$-PEI/PEEK powders (shown Fig. 12c and d), the addition of WS$_2$ nanoparticle did not affect the crystallisation temperature, but enhanced slightly the rate of crystallisation by providing a shaper onset of crystallisation. Previous studies showed that presence of low concentrations of WS$_2$ have a nucleating effect, increasing crystallisation temperature. But the effect disappeared at higher loadings. The authors [41,42] concluded that the higher concentrations of IF-WS$_2$ retard the diffusion and rearrangement of the long polymer chains and therefore decrease the degree of crystallisation. However, the crystallisation mechanisms here are more complex for two reasons: 1) the presence of an additional polymer—PEI, known to influence the crystallisation of PEEK due to its amorphous structure; 2) the nanoparticles and PEI are not mechanically melt compounded within the PEEK polymer matrix or solvent cast to allow good polymer chain diffusion and therefore the influence of the nanoparticles on the PEEK structure is expected to be less intense.

3.3. Powder rheology test of PEI coated PEEK and its nanocomposites

Only WS$_2$ nanocomposite powder was further investigated for flow characteristics. Fig. 13 shows the digital images of 1WS$_2$-PEEK, 5WS$_2$-PEEK (dry mixtures), 1WS$_2$-PEI/PEEK, and 5WS$_2$-PEI/PEEK powders. The coloration is clearly different between the dry mixed and WS$_2$ core-shell powders. The dry mixed samples remain white/cream, the typical colour of PEEK 150 PF, where as the WS$_2$-PEI/PEEK powder developed a greyish colour, indicating the presence of well-dispersed WS$_2$.

Stability and Flow Rate tests were carried out for PEEK and WS$_2$-PEEK dry mixtures and WS$_2$-PEI/PEEK core-shell powders. The results are reported in Table 2. The BFE value for PEK HP3 is the highest found for the materials in this study, requiring approximately 182 mJ of energy to displace the powder at each rotation; the second highest BFE value is for PEI/PEEK, with 161 mJ. These two powders showed the highest Conditioned Bulk Density (CBD) as well. A higher CBD is the result of higher particle density and good packing. Such particles require higher energy to displace them and therefore higher BFE. High CBD and BFE values are characteristics of a powder with good flowability [43,44]. During the downward movement of the blade, the particles are forced to flow at the blade surface and cover the air gaps that exist in between the particles creating a relatively short and localized stress transmission zone, which increases BFE.

When normalized by their respective CBD, PEK HP3 still displays the highest BFE, followed by PEI/PEEK, which suggests that PEK HP3 is flowing better not only as a result of its density but also due to a low cohesive effect as more particles were being displaced by the blade simultaneously. The lowest values of BFE were found for 1WS$_2$-PEEK and 5WS$_2$-PEEK dry mixtures, which also present the lowest values of CBD (both 0.34 g/ml). This suggests that the nanoparticles created voids in the bulk. The SEM images of PEK HP3 and the dry mixtures are
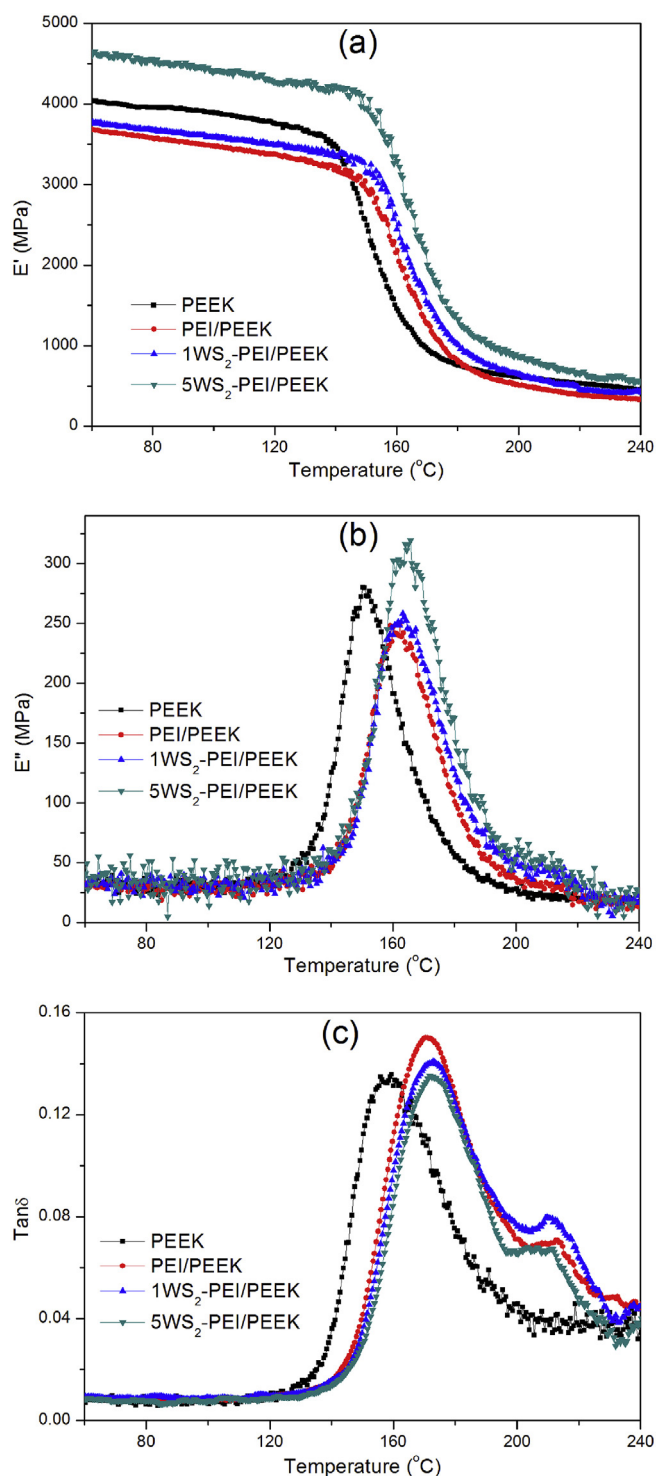
Fig. 15. Thermal mechanical behaviour of hot-compressed films.

shown in Fig. S2.

The values of SE oppose the results achieved with BFE. As shown in Table 2, WS$_2$-PEEK dry mix powders show a lower SE than plain PEEK and PEI/PEEK, which suggests that WS$_2$-PEEK dry mix powders are more easily lifted by the blade when in a low stress environment than PEEK and PEI/PEEK. The BFE values reported in Table 2 show that an application of pressure may change flow performance as other factors like packing and consolidation are of major importance. The measurement of SE, however, was performed in an unstressed and unconfined bed, therefore a direct indication of shearing and friction forces acting

in the system. The addition of nanoparticles into the matrix powders seems to reduce SE by creating voids which act as a barrier to friction between particles.

Although lower values of SE are found for WS$_2$-PEEK dry mixtures, all the powders presented a moderate cohesion, even 5WS$_2$-PEI/PEEK which shows the highest value of SE from all materials analysed. PEK HP3 shows the second highest SE value, followed by 1WS$_2$-PEI/PEEK, PEEK and PEI/PEEK. The addition of nanoparticles seems to increase SE when coated with PEI but to decrease SE when PEI is not present, which suggests the effectiveness of PEI shell structure.

Regarding uniformity throughout the bulk, all powders are quite stable and the results of SI are consistent except for 5WS$_2$-PEI/PEEK, which shows a relatively high standard deviation as observed in Fig. 14 with the increase in energy during test 3 and a linear increase from test 5. The reason for this larger variation in SI is probably due to the aggregation of WS$_2$ nanoparticles.

The powder rheology properties of PEI/PEEK and its WS$_2$ nanocomposite powders were overall improved by the PEI shell, making the new nanocomposite powders comparable in performance with the commercial laser sintering grade, EOS HP3 PEK.

3.4. Dynamic thermo-mechanical analysis

The DMTA results of hot-compression moulded samples of pure PEEK, PEI/PEEK, 1WS$_2$-PEI/PEEK, and 5WS$_2$-PEI/PEEK are shown in Fig. 15a–c. The storage modulus provides information related with the stiffness of the nanocomposites as a function of temperature. The storage modulus (E′) of pure PEEK was identified as approximately 3.9 GPa at 100 °C, in agreement with the literature values [45]. The storage modulus of the PEI/PEEK is slightly lower than the values of pure PEEK across the entire temperature range, which is consistent with the lower degree of crystallisation calculated in PEI/PEEK samples and presented in Table 1. The incorporation of the WS$_2$ nanoparticle in PEI/PEEK matrix led to higher storage moduli in comparison with PEI/PEEK, suggesting a stiffening effect [46]. The 5WS$_2$-PEI/PEEK sample showed a 27% increase in E′ at 100 °C, and 70% improved at 200 °C. The E′ improvement attained with the addition of WS$_2$ can be attributed to a reinforcement effect [38,46]. The two materials (PEI and WS$_2$) added to main PEEK particles seem to have an opposite effect: the PEI tends to lower the crystallinity and storage modulus whereas WS$_2$ nanoparticles tend to activate the crystallisation and increase the storage modulus. Overall, for the proposed concentrations, the WS$_2$-PEI/PEEK powders created structures with enhanced mechanical performance.

The tan δ gives a measure of the damping properties within the material. As shown in Fig. 15c, pure PEEK has a relaxation at approximately 158 °C, corresponding to the T$_g$. As the PEI/PEEK is a melt miscible blend, one glass transition temperature is generally reported, with many studies defining the T$_g$ of PEI/PEEK blends from DSC traces as one transition [31]. Surprisingly, in this study, two well-defined transitions were observed at 171 and 213 °C. It is believed that this is the result of the crystallisation mechanism, the lower peak corresponding to the relaxation of PEEK and the higher one corresponding to PEI. Several studies proved that the PEI segregates within PEEK in three modes: (1) inter-lamellar; (2) inter-lamellar bundles; (3) inter-spherulitic [47,48]. As the two polymers are not mechanically blended (injection moulded) or solvent cast to allow a good inter-penetration and diffusion of the two polymeric chains within each other (PEI being only coated on the surface of PEEK particles), it is possible that the PEI is rejected from the individual PEEK lamellae, the inter-spherulitic mode becoming the predominant method of separation of PEI. In such case, the blend would have large PEI rich regions and therefore could retain two glass transition temperatures.

The shift in T$_g$ in the case of 1WS$_2$-PEI/PEEK and 5WS$_2$-PEI/PEEK is small in comparison with PEI/PEEK (3 °C), however it suggests a good dispersion and adhesion of WS$_2$ particles with the polymer matrix [42]. In addition, a gradual drop in the height of tan δ peak is found with the

increasing WS$_2$ content. This is due to the reduction in mobility of the polymer caused by the addition of nanoparticles.

4. Conclusions

A new method for preparing nanocomposite powders based on a core-shell structure was successfully developed. A PEI polymeric coating with PEEK core powder; and two types of nanoparticles, GNP and IF-WS$_2$, with different concentrations were studied. The surface morphology was observed by SEM, confirming a relatively homogenous distribution of the nanoparticles within the coating layer at lower concentration (0.1 and 1 wt%), but the nanoparticles tend to aggregate at higher nanoparticles concentration (5 wt%). TEM images of cross-section area of composite powders confirmed the formation of core-shell structure, where the nanoparticles with various concentrations were embedded into the shell. The PEI/PEEK core-shell powders exhibited improved powder rheology properties compared with the plain PEK and PEEK grades, an advantage for the laser sintering. The DMTA results of the nanocomposites showed an overall increase in the mechanical performance with PEI and nanoparticles having opposite effects on the crystallisation of PEEK. This method provides a new strategy for the homogeneous incorporation of nanoparticles into a polymer matrix with potential use in two manufacturing processes: laser sintering and hierarchical composite manufacture.

Acknowledgements

Appendix A. Supplementary data

Supplementary data to this article can be found online at https://doi.org/10.1016/j.compscitech.2018.11.046.

References

[1] M. Bhattacharya, Polymer nanocomposites—a comparison between carbon nanotubes, graphene, and clay as nanofillers, Materials 9 (2016) 262.

[2] E.W. Wong, P.E. Sheehan, C.M. Lieber, Nanobeam mechanics: elasticity, strength, and toughness of nanorods and nanotubes, Science 277 (1997) 1971–1975.

[3] M.F. Yu, O. Lourie, M.J. Dyer, K. Moloni, T.F. Kelly, R.S. Ruoff, Strength and breaking mechanism of multiwalled carbon nanotubes under tensile load, Science 287 (2000) 637–640.

[4] C. Lee, X. Wei, J.W. Kysar, J. Hone, Measurement of the elastic properties and intrinsic strength of monolayer graphene, Science 321 (2008) 385–388.

[5] A.K. Geim, K.S. Novoselov, The rise of graphene, Nat. Mater. 6 (2007) 183–191.

[6] A.A. Balandin, S. Ghosh, W. Bao, I. Calizo, D. Teweldebrhan, F. Miao, C.N. Lau, Superior thermal conductivity of single-layer graphene, Nano Lett. 8 (2008) 902–907.

[7] K. Thummavichai, Y. Xia, Y. Zhu, Recent progress in chromogenic research of tungsten oxides towards energy-related applications, Prog. Mater. Sci. 88 (2017) 281–324.

[8] F. Xu, T. Kobayashi, Z. Yang, T. Sekine, H. Chang, N. Wang, Y. Xia, Y. Zhu, How the toughest inorganic fullerene cages absorb shockwave pressures in a protective nanocomposite: experimental evidence from two in situ investigations, ACS Nano 11 (2017) 8114–8121.

[9] M. Tanahashi, Development of fabrication methods of filler/polymer nanocomposites: with focus on simple melt-compounding-based approach without surface modification of nanofillers, Materials 3 (2010) 1593.

[10] P. Hornsby, Compounding of particulate-filled thermoplastics, in: S. Palsule (Ed.), Polymers and Polymeric Composites: a Reference Series, Springer Berlin Heidelberg, Berlin, Heidelberg, 2016, pp. 1–16.

[11] F. Yang, G.L. Nelson, Polymer/silica nanocomposites prepared via extrusion, Polym. Adv. Technol. 17 (2006) 320–326.

[12] K. Kalaitzidou, H. Fukushima, L.T. Drzal, A new compounding method for exfoliated graphite–polypropylene nanocomposites with enhanced flexural properties and lower percolation threshold, Compos. Sci. Technol. 67 (2007) 2045–2051.

[13] B. Chen, Y. Wang, S. Berretta, O. Ghita, Poly Aryl Ether Ketones (PAEKs) and carbon-reinforced PAEK powders for laser sintering, J. Mater. Sci. 52 (2017) 6004–6019.

[14] N. Mys, R. Van De Sande, A. Verberckmoes, L. Cardon, Processing of polysulfone to free flowing powder by mechanical milling and spray drying techniques for use in selective laser sintering, Polymers 8 (2016) 150.

[15] R. Krishnamoorti, Strategies for dispersing nanoparticles in polymers, MRS Bull. 32 (2007) 341–347.

[16] C. Zhi, Y. Bando, C. Tang, R. Xie, T. Sekiguchi, D. Golberg, Perfectly dissolved boron nitride nanotubes due to polymer wrapping, J. Am. Chem. Soc. 127 (2005) 15996–15997.

[17] A. Star, D.W. Steuerman, J.R. Heath, J.F. Stoddart, Starched carbon nanotubes, Angew. Chem. Int. Ed. 41 (2002) 2508–2512.

[18] J. Pyun, K. Matyjaszewski, Synthesis of nanocomposite organic/inorganic hybrid materials using Controlled/"Living" radical polymerization, Chem. Mater. 13 (2001) 3436–3448.

[19] X. Liang, R. Stacey, T. Mahesh, R. Jiaxiang, A.S. Devon, K. Ramanan, Structure and melt rheology of polystyrene-based layered silicate nanocomposites, Nanotechnology 16 (2005) S514.

[20] S.H. Sajjadi Jazi, M. Nasr Esfahany, R. Bagheri, Investigation of the addition of nano-CaCo3 at dry mixing or onset of fusion on the dispersion, torque, and mechanical properties of compounded PVC, J. Vinyl Addit. Technol. 18 (2012) 153–160.

[21] J.J. Dongyu Cai, Mo Song, WO2009/034361, in, 2007.

[22] J. Bai, R.D. Goodridge, R.J.M. Hague, M. Song, Improving the mechanical properties of laser-sintered polyamide 12 through incorporation of carbon nanotubes, Polym. Eng. Sci. 53 (2013) 1937–1946.

[23] J. Bai, R.D. Goodridge, R.J.M. Hague, H. Murakami, Nanostructural characterization of carbon nanotubes in laser-sintered polyamide 12 by 3D-TEM, J. Mater. Res. 29 (2014) 1817–1823.

[24] J. Bai, R.D. Goodridge, R.J.M. Hague, M. Song, M. Okamoto, Influence of carbon nanotubes on the rheology and dynamic mechanical properties of polyamide-12 for laser sintering, Polym. Test. 36 (2014) 95–100.

[25] H. Qian, E.S. Greenhalgh, M.S.P. Shaffer, A. Bismarck, Carbon nanotube-based hierarchical composites: a review, J. Mater. Chem. 20 (2010) 4751–4762.

[26] A.M. Díez-Pascual, M. Naffakh, Polypropylene/glass fiber hierarchical composites incorporating inorganic fullerene-like nanoparticles for advanced technological applications, ACS Appl. Mater. Interfaces 5 (2013) 9691–9700.

[27] M. Aurilia, L. Sorrentino, F. Berardini, S. Sawalha, S. Iannace, Mechanical properties of nano/micro multilayered thermoplastic composites based on PP matrix, J. Thermoplast. Compos. Mater. 25 (2012) 835–849.

[28] S. Padaki, L.T. Drzal, A simulation study on the effects of particle size on the consolidation of polymer powder impregnated tapes, Composites Part A 30 (1999) 325–337.

[29] F. Xu, T.P. Almeida, H. Chang, Y. Xia, M.L. Wears, Y. Zhu, Multi-walled carbon/IF-WS2 nanoparticles with improved thermal properties, Nanoscale 5 (2013) 10504–10510.

[30] A.R. McLauchlin, O.R. Ghita, Studies on the thermal and mechanical behavior of PLA-PET blends, J. Appl. Polym. Sci. 133 (2016) (n/a-n/a).

[31] G. Crevecoeur, G. Groeninckx, Binary blends of poly(ether ether ketone) and poly (ether imide): miscibility, crystallization behavior and semicrystalline morphology, Macromolecules 24 (1991) 1190–1195.

[32] S. Berretta, Y. Wang, R. Davies, O.R. Ghita, Polymer viscosity, particle coalescence and mechanical performance in high-temperature laser sintering, J. Mater. Sci. 51 (2016) 4778–4794.

[33] Y. Wang, D. Rouholamin, R. Davies, O.R. Ghita, Powder characteristics, microstructure and properties of graphite platelet reinforced poly ether ether ketone composites in high temperature laser sintering (HT-LS), Mater. Des. 88 (2015) 1310–1320.

[34] H.L. Chen, R.S. Porter, Phase and crystallization behavior of solution-blended poly (ether ether ketone) and poly(ether imide), Polym. Eng. Sci. 32 (1992) 1870–1875.

[35] J. Chen, Q. Guo, Z. Zhao, X. Wang, C. Duan, Structures and mechanical properties of PEEK/PEI/PES plastics alloys blent by extrusion molding used for cable insulating jacketing, Procedia Eng. 36 (2012) 96–104.

[36] P.C. Dawson, D.J. Blundell, X-ray data for poly(aryl ether ketones), Polymer 21 (1980) 577–578.

[37] B. Yazdani, Y. Xia, I. Ahmad, Y. Zhu, Graphene and carbon nanotube (GNT)-reinforced alumina nanocomposites, J. Eur. Ceram. Soc. 35 (2015) 179–186.

[38] N. Wang, Z. Yang, K. Thummavichai, F. Xu, C. Hu, H. Chen, Y. Xia, Y. Zhu, Novel graphitic carbon coated IF-WS2 reinforced poly(ether ether ketone) nanocomposites, RSC Adv. 7 (2017) 35265–35273.

[39] B. Chen, S. Berretta, K. Evans, K. Smith, O. Ghita, A primary study into graphene/polyether ether ketone (PEEK) nanocomposite for laser sintering, Appl. Surf. Sci. 428 (2018) 1018–1028.

[40] J.R. Potts, D.R. Dreyer, C.W. Bielawski, R.S. Ruoff, Graphene-based polymer nanocomposites, Polymer 52 (2011) 5–25.

[41] A.M. Díez-Pascual, M. Naffakh, C. Marco, G. Ellis, M.A. Gómez-Fatou, High-performance nanocomposites based on polyetherketones, Prog. Mater. Sci. 57 (2012) 1106–1190.

[42] M. Naffakh, A.M. Díez-Pascual, C. Marco, M.A. Gómez, I. Jiménez, Novel melt-processable poly(ether ether ketone)(PEEK)/Inorganic fullerene-like WS2 nanoparticles for critical applications, J. Phys. Chem. B 114 (2010) 11444–11453.

[43] S. Ziegelmeier, F. Wöllecke, C. Tuck, R. Goodridge, R. Hague, Characterizing the bulk & flow behaviour of LS polymer powders, Proceedings SFF Symposium, Austin (TX), USA, 2013.

[44] M. Leturia, M. Benali, S. Lagarde, I. Ronga, K. Saleh, Characterization of flow properties of cohesive powders: a comparative study of traditional and new testing

methods, Powder Technol. 253 (2014) 406–423.

[45] V.P. 150PF, https://www.victrex.com/~/media/datasheets/victrex_tds_150pf.pdf, (2016).

[46] A.M. Díez-Pascual, A.L. Díez-Vicente, Nano-TiO2 reinforced PEEK/PEI blends as biomaterials for load-bearing implant applications, ACS Appl. Mater. Interfaces 7 (2015) 5561–5573.

[47] S.D. Hudson, D.D. Davis, A.J. Lovinger, Semicrystalline morphology of poly(aryl ether ether ketone)/poly(ether imide) blends, Macromolecules 25 (1992) 1759–1765.

[48] A.M. Jonas, D.A. Ivanov, D.Y. Yoon, The Semicrystalline Morphology of Poly (ether−ether−ketone) Blends with Poly(ether−imide), Macromolecules 31 (1998) 5352–5362.